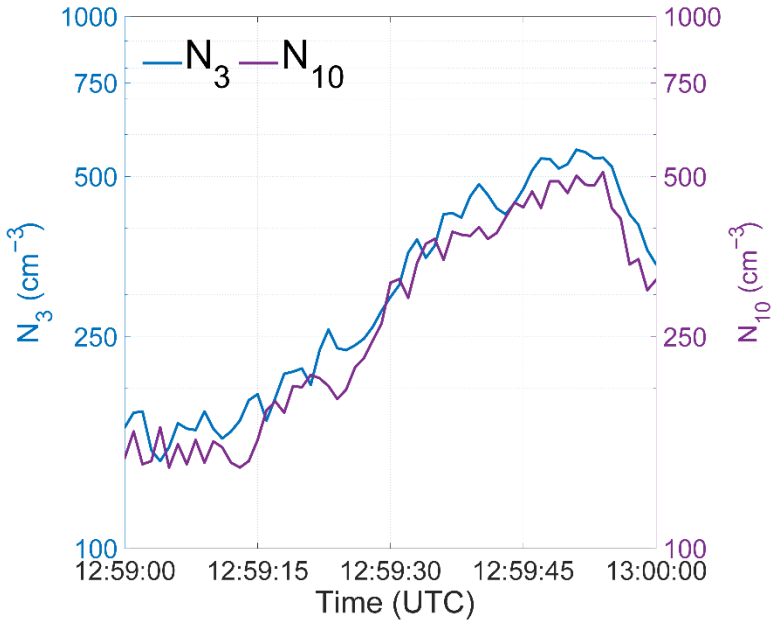

Figure S1. Time series of particle number concentrations for particles >3 nm and >10 nm measured by the ultrafine and fine CPCs, respectively.

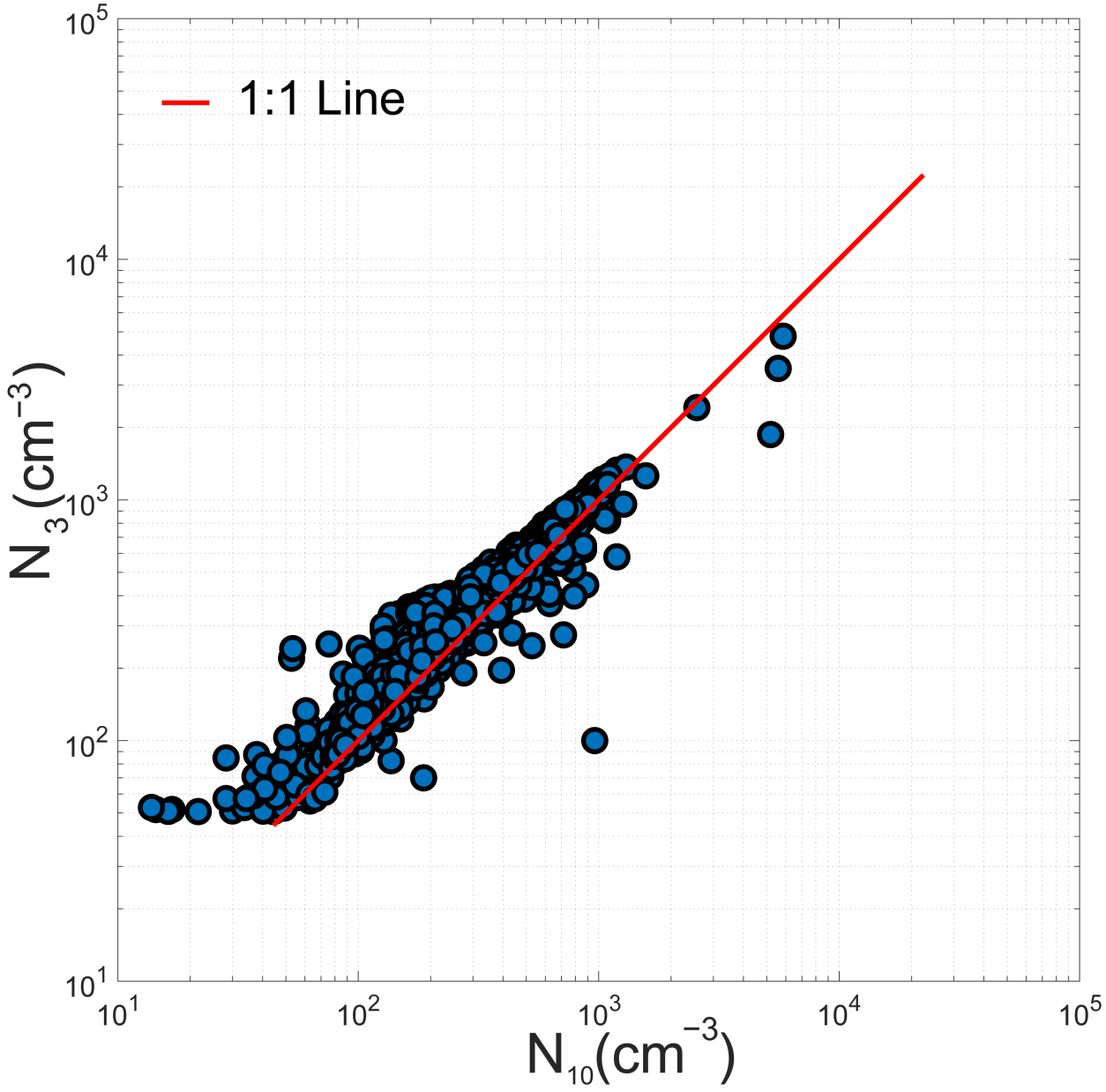

Figure S2. Scatter plot of particle number concentrations for particles greater than 3 nm versus those greater than 10 nm.

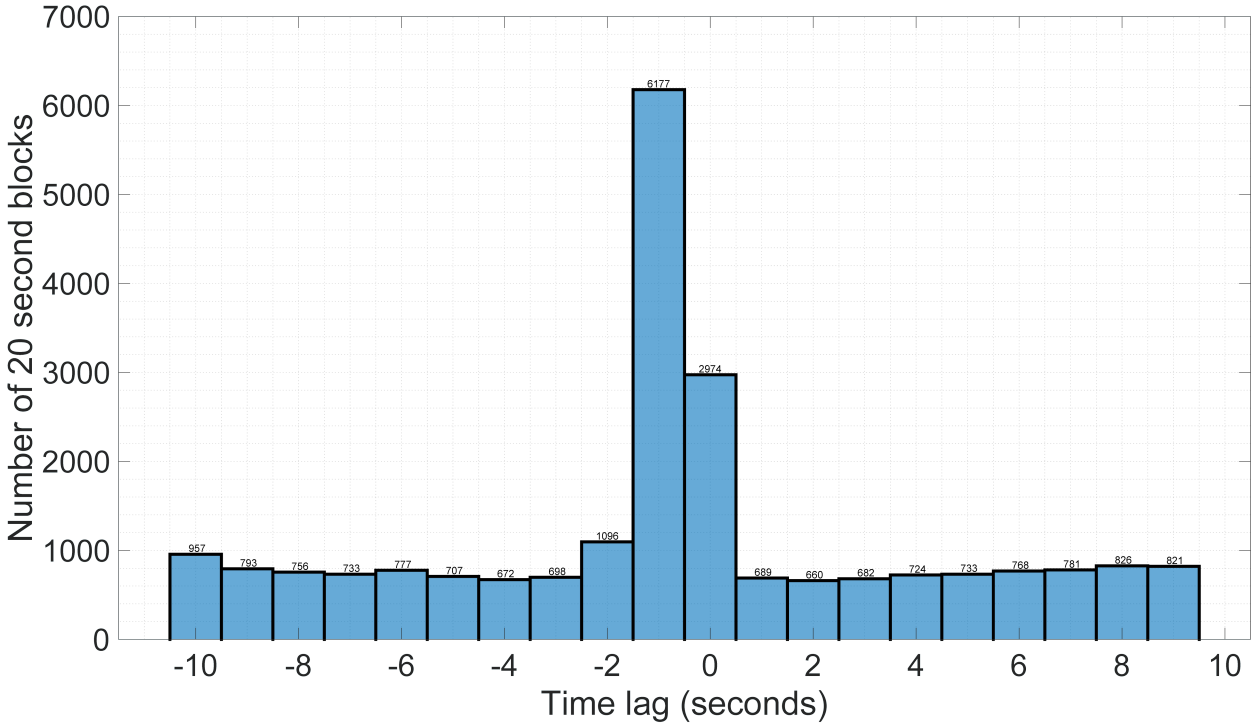

Figure S3. Frequency distribution of temporal delays between ultrafine and fine CPCs.

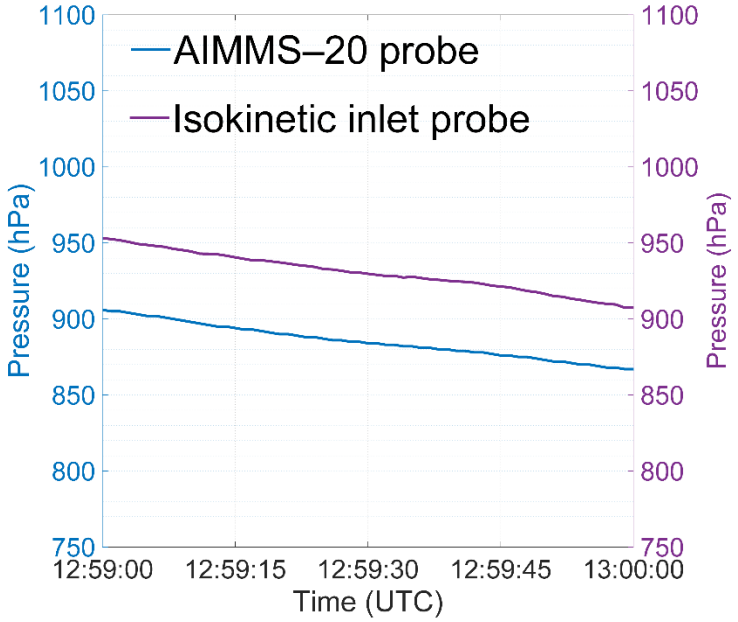

Figure S4. Time series of pressure recorded at the isokinetic inlet and by the Rosemount 1201F1 pressure sensor mounted on the AIMMS–20 probe.

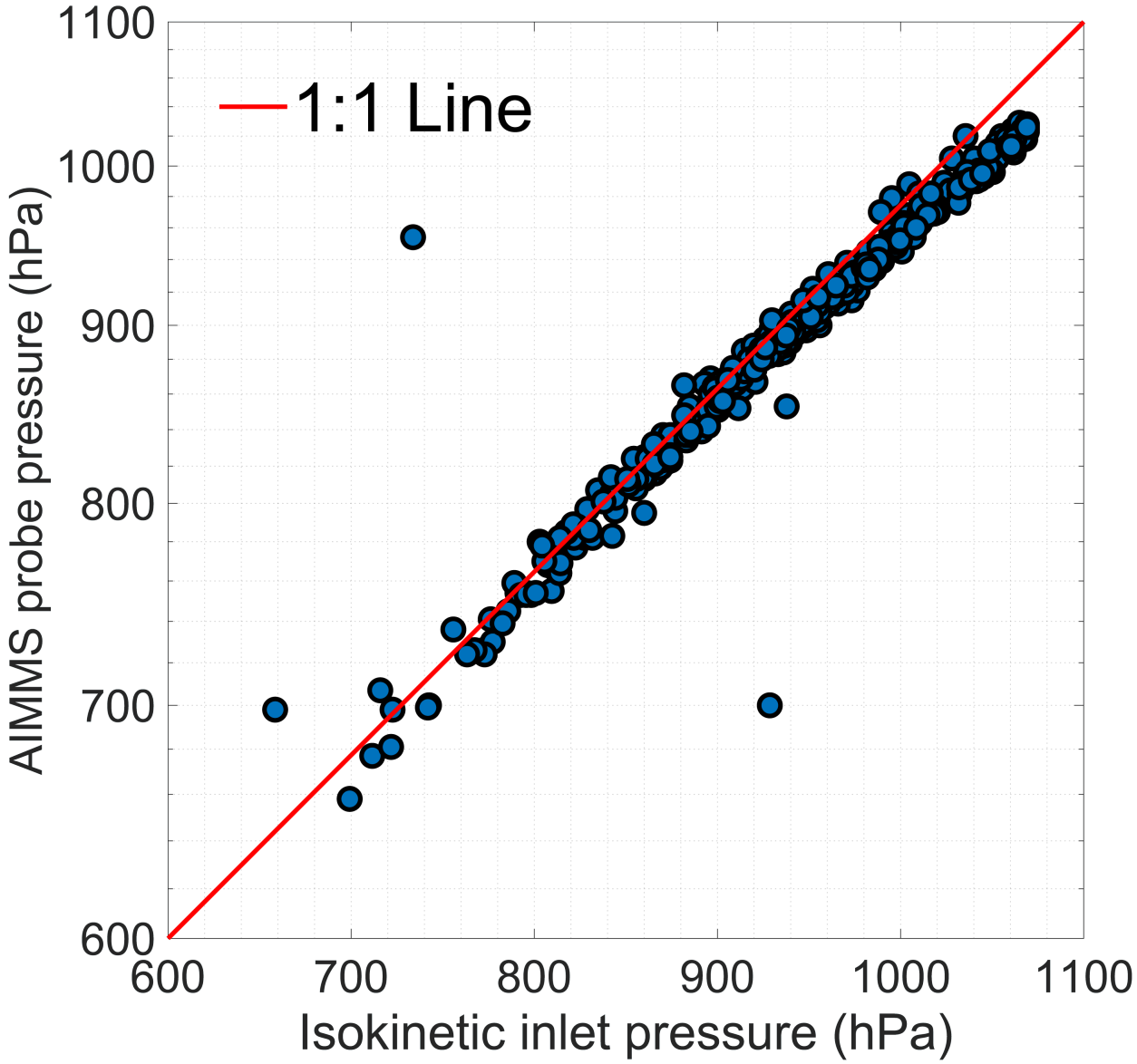

Figure S5. Scatter plot of pressure measurements from the Rosemount 1201F1 sensor attached to the AIMMS–20 probe vs those at the isokinetic inlet.

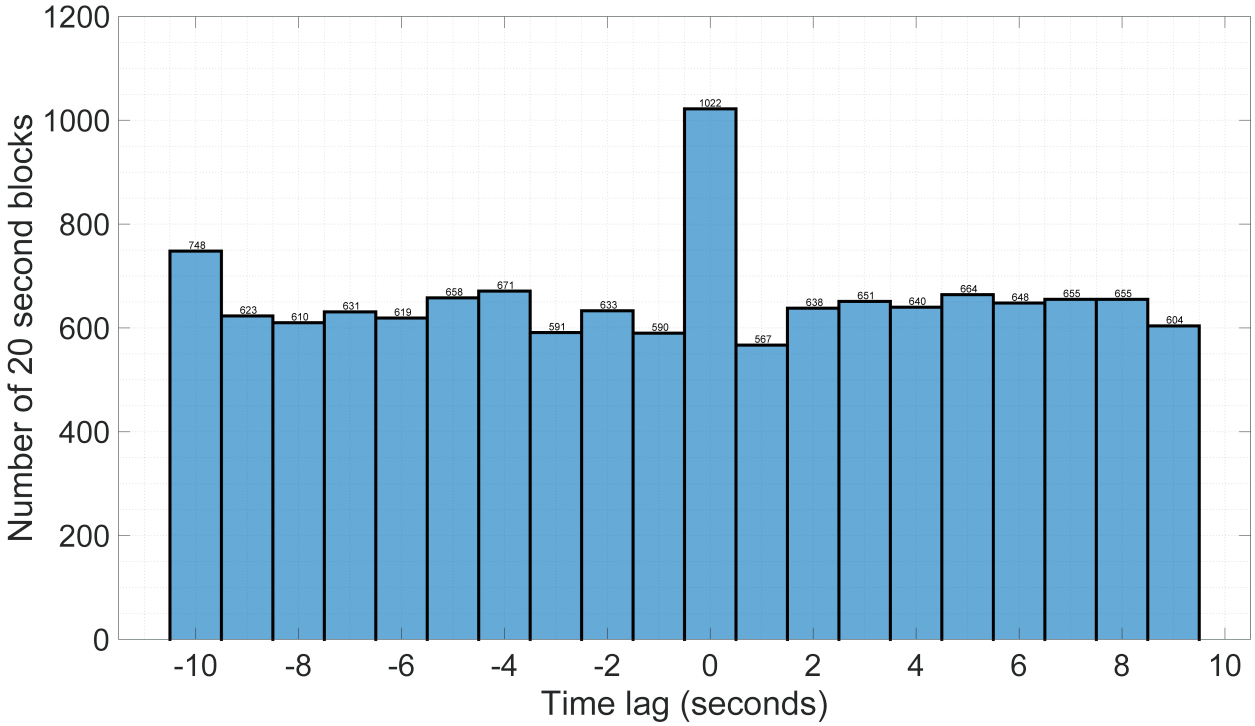

Figure S6. Frequency distribution of temporal delays between isokinetic and AIMMS–20 inlet measurements calculated using the covariance maximization method across the entire campaign.

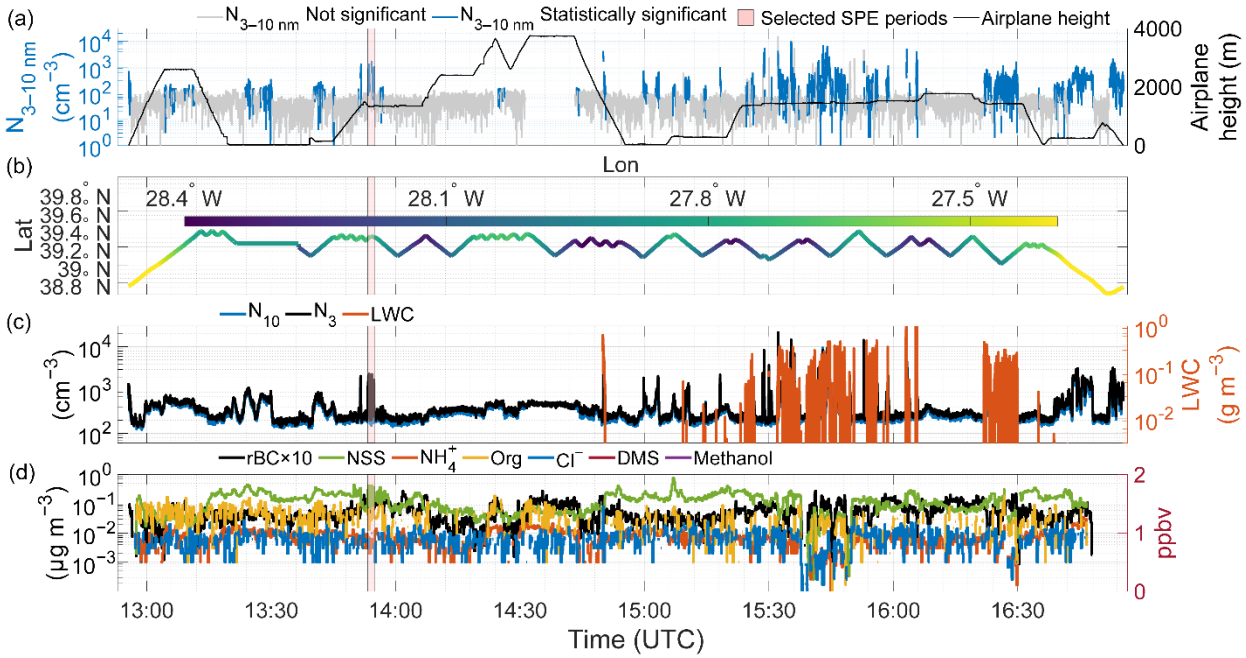

Figure S7. Multi-parameter time series analysis during the February 10, 2018 flight showing: (a) $N_{3\text{-}10}$ particle concentrations with aircraft altitude (b) aircraft position showing latitude and longitude (c) particle number concentrations for N_{10}, N_3, and liquid water content (LWC); and (d) non-refractory aerosol chemical composition including non-seasalt sulfate (NSS), ammonium ion (NH_4^+), organics (Org), and chlorine ion (Cl^-), plus refractory black carbon (rBC, multiplied by 10 for visualization) in μg m^{-3}, and trace gas concentrations of dimethylsulfide (DMS) and methanol in ppbv.

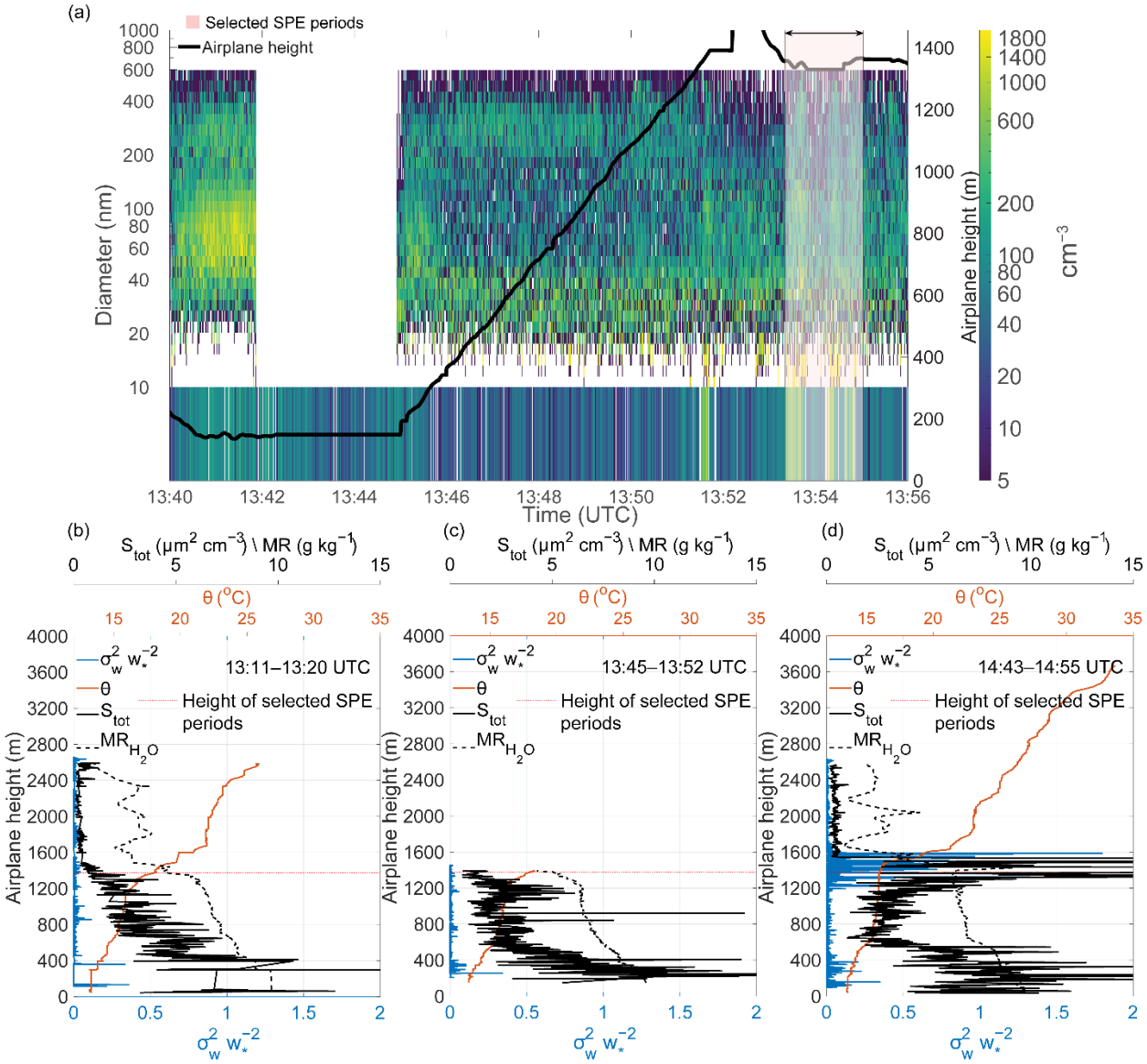

Figure S8. (a) The main panel shows size-resolved particle number concentrations (10-600 nm diameter) from FIMS as a function of time and altitude, while $N_{3\text{-}10}$ concentrations are displayed in the lower strip. Colors represent particle number concentrations (cm^{-3}) according to the scale bar. Gaps in the time series indicate the missing data. (b-d) Vertical profiles of potential temperature (θ), normalized vertical velocity variance ($\sigma_w^2\, w_*^{-2}$), particle total surface area (Stot), and water vapor mixing ratio (MR).

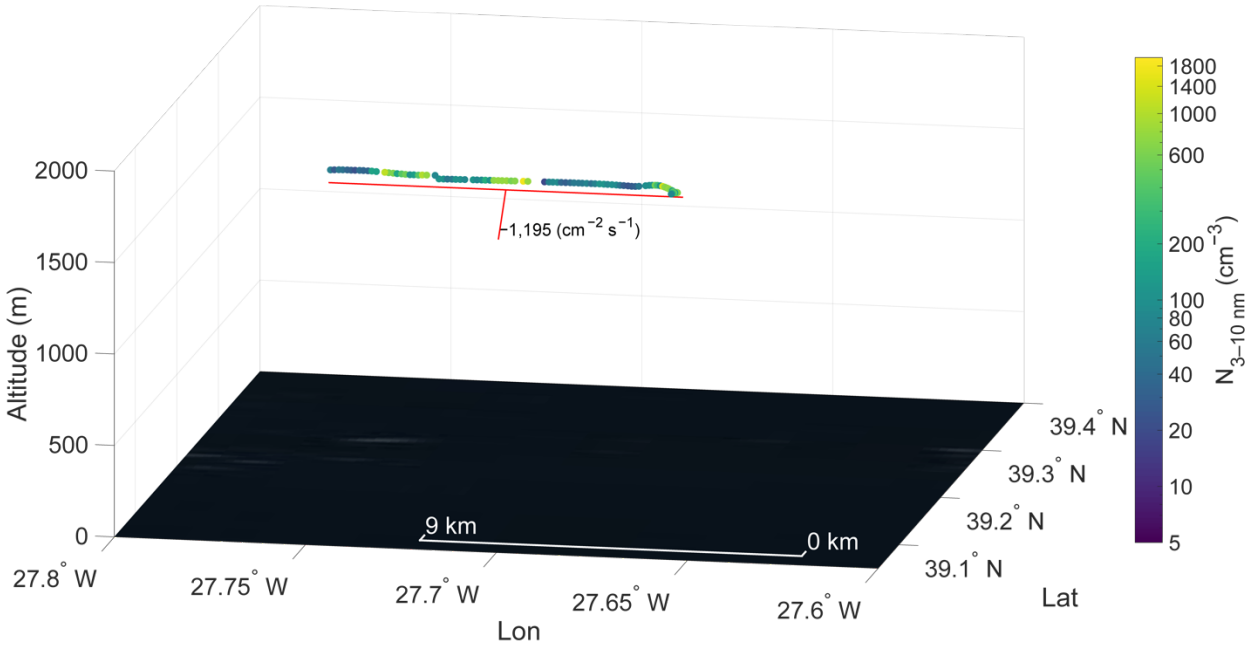

Figure S9. Spatial distribution of $N_{3\text{-}10}$ particle concentrations along the flight track during the period highlighted in Figures S7 and S8. Mean calculated fluxes are labeled on the track. Color scale indicates particle number concentrations (cm^{-3}). The background shows a satellite-corrected reflectance image taken from the overpass at 14:25 UTC, with the ocean surface appearing dark and clouds appearing white, Credit: NASA Worldview Snapshots.

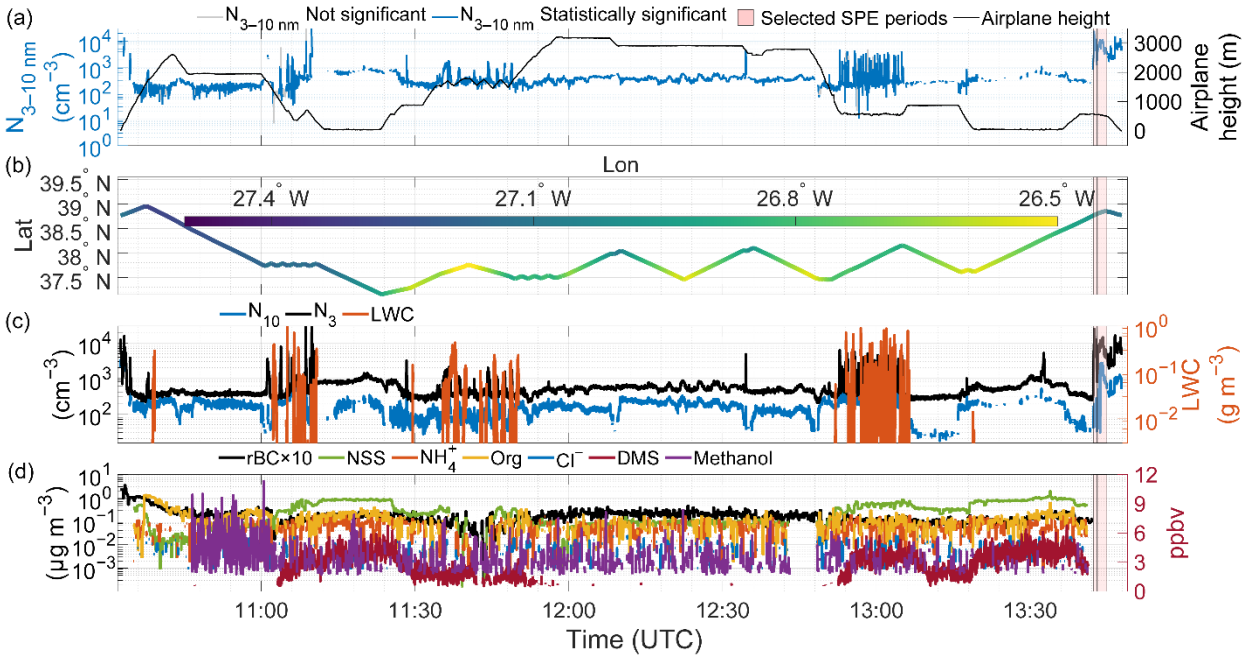

Figure S10. Multi-parameter time series analysis during the July 07, 2017 flight showing: (a) $N_{3–10}$ particle concentrations with aircraft altitude (b) aircraft position showing latitude and longitude (c) particle number concentrations for N_{10}, N_3, and liquid water content (LWC); and (d) non-refractory aerosol chemical composition including non–seasalt sulfate (NSS), ammonium ion (NH_4^+), organics (Org), and chlorine ion (Cl^-), plus refractory black carbon (rBC, multiplied by 10 for visualization) in μg m^{-3}, and trace gas concentrations of dimethylsulfide (DMS) and methanol in ppbv.

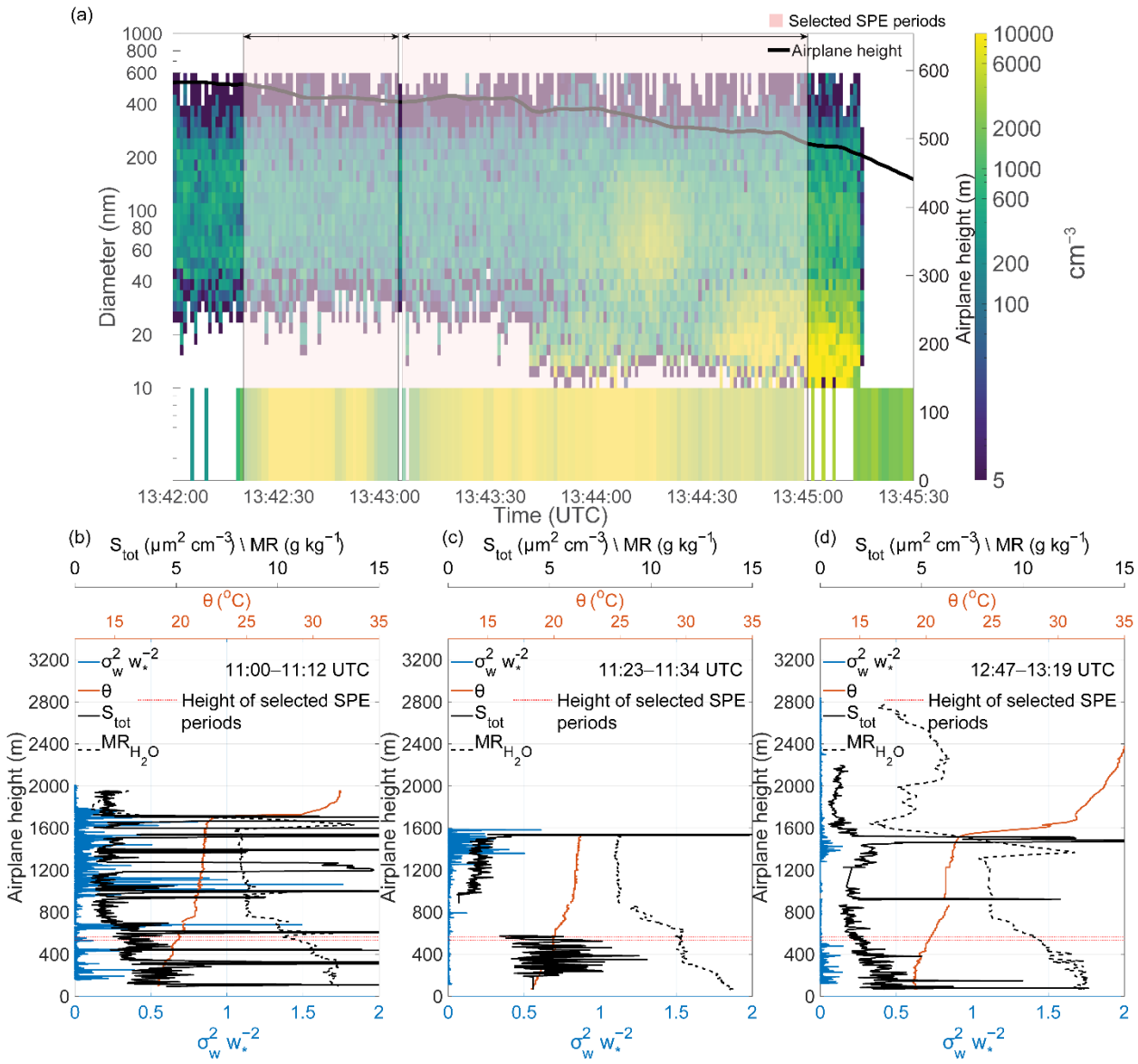

Figure S11. (a) The main panel shows size-resolved particle number concentrations (10–600 nm diameter) from FIMS as a function of time and altitude, while $N_{3\text{-}10}$ concentrations are displayed in the lower strip. The black line indicates aircraft altitude. Colors represent particle number concentrations (cm^{-3}) according to the scale bar. Gaps in the time series indicate the missing data. (b-d) Vertical profiles of potential temperature (θ), normalized vertical velocity variance ($\sigma_w^2 w_*^{-2}$), particle total surface area (Stot), and water vapor mixing ratio (MR).

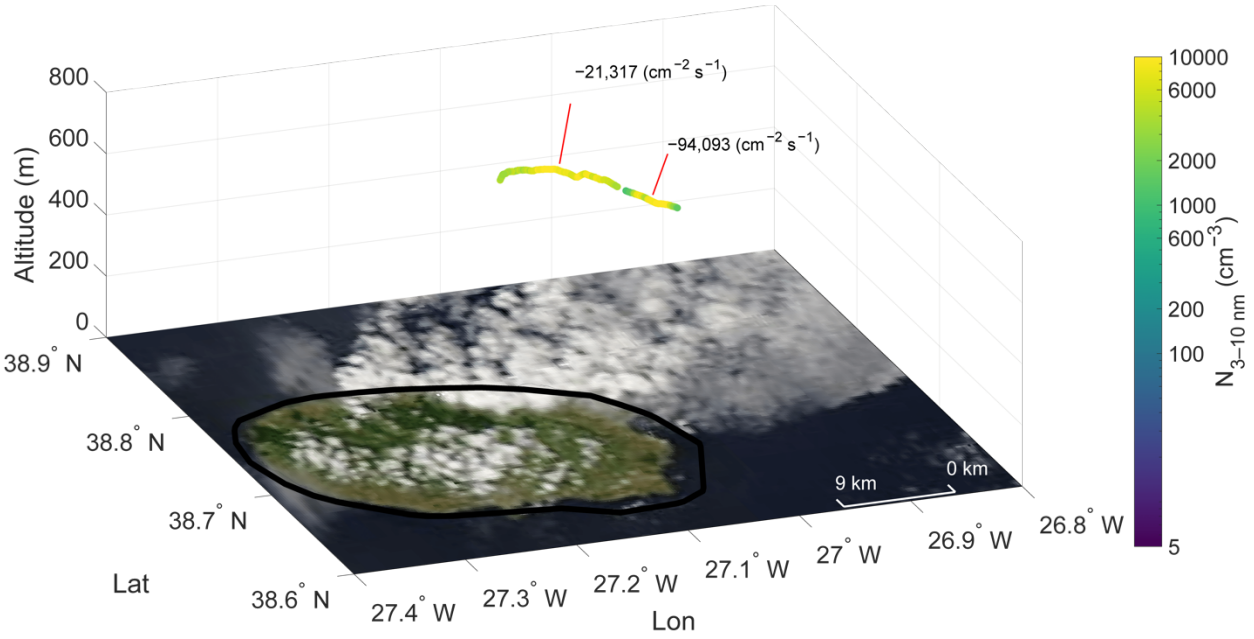

Figure S12. Spatial distribution of $N_{3–10}$ particle concentrations along the flight track during the period highlighted in Figures S10 and S11. Mean calculated fluxes are labeled on the track. Color scale indicates particle number concentrations (cm^{-3}). The background shows a satellite-corrected reflectance image taken from the overpass at 15:02 UTC with the ocean surface appearing dark and clouds appearing white, Credit: NASA Worldview Snapshots.

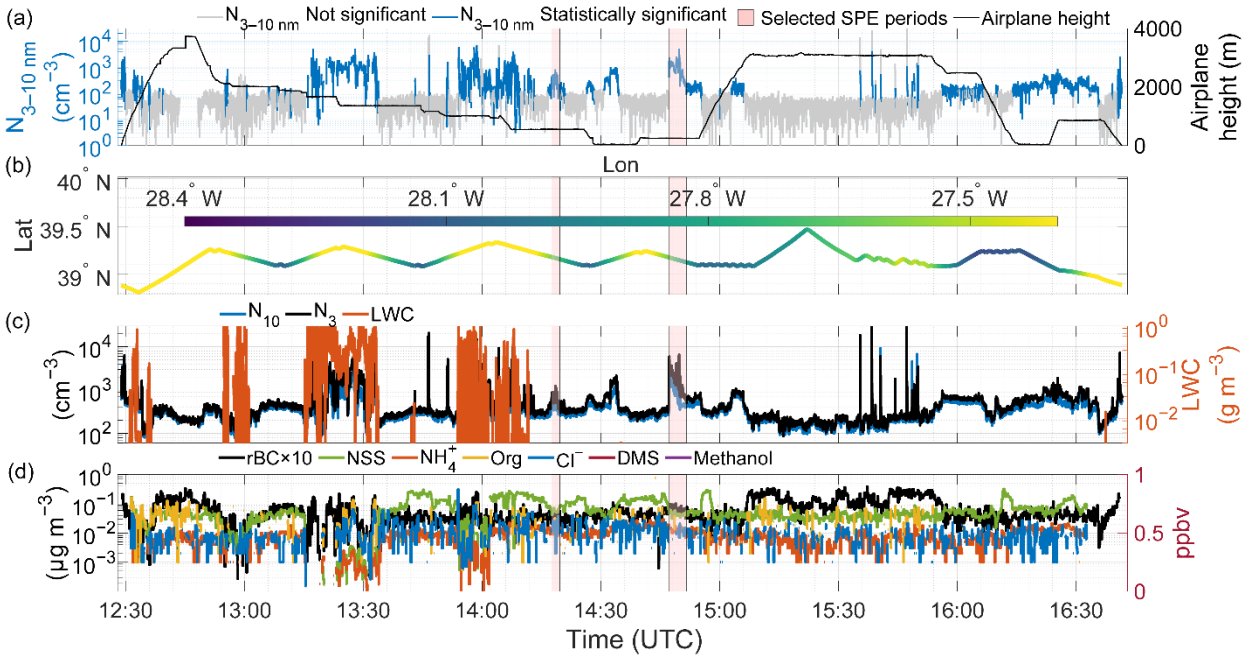

Figure S13. Multi–parameter time series analysis during the February 18, 2018 flight showing: (a) $N_{3\text{-}10}$ particle concentrations with aircraft altitude (b) aircraft position with latitude and longitude; (c) particle number concentrations for N_{10}, N_3, and liquid water content (LWC); and (d) non-refractory aerosol chemical composition (non–seasalt sulfate, NSS, ammonium ion, NH_4^+, organics, Org, and chlorine ion, Cl^-) and rBC (multiplied by 10 for visual representation) in μg m^{-3} from aerosol mass spectrometer measurements, and trace gas concentrations of dimethylsulfide, DMS and methanol in ppbv.

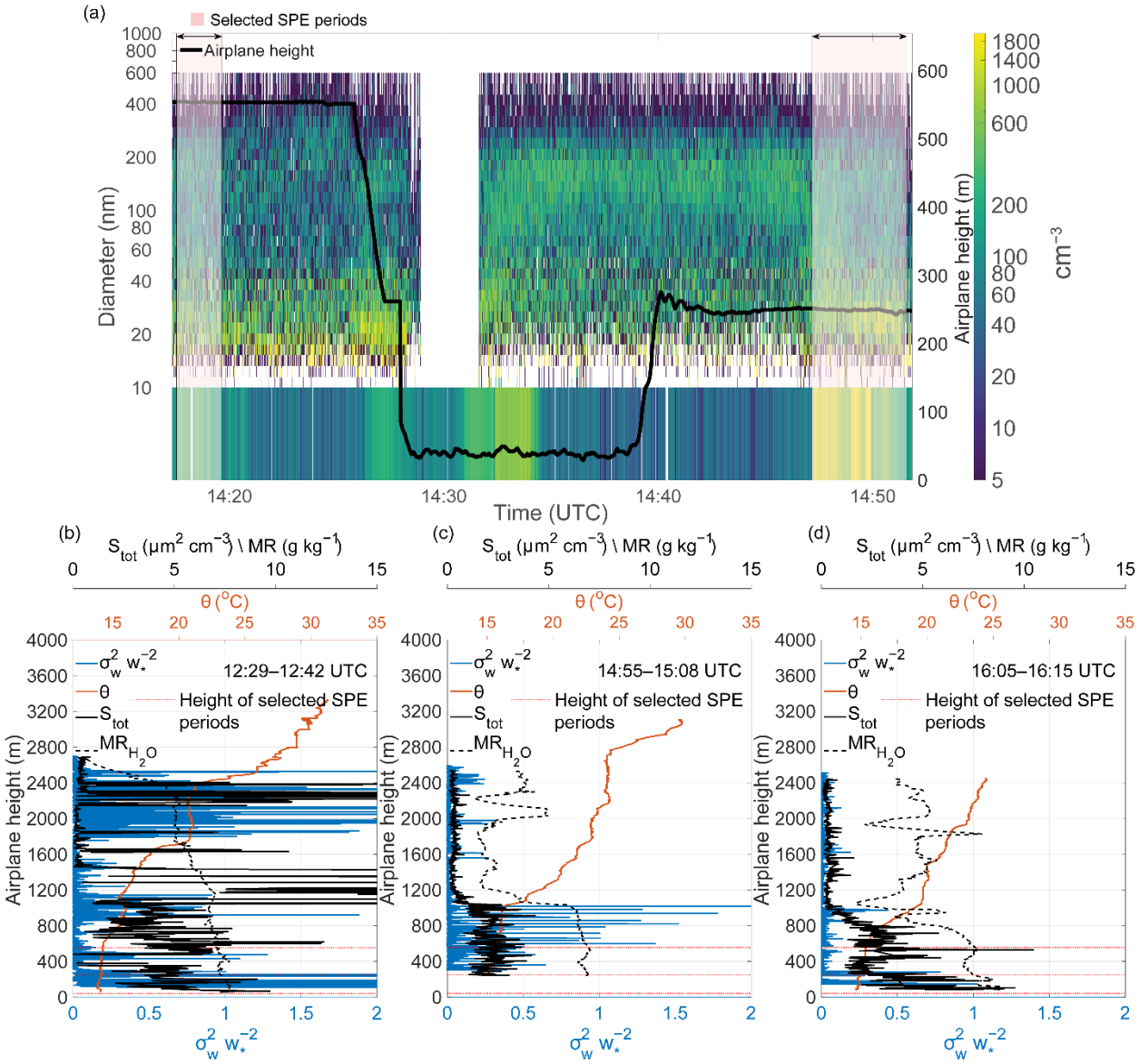

Figure S14. (a) The main panel shows size-resolved particle number concentrations (10–600 nm diameter) from FIMS as a function of time and altitude, while N_{3-10} concentrations are displayed in the lower strip. Pink shading is the same as in Figure S13. Colors represent particle number concentrations (cm^{-3}) according to the scale bar. Gaps in the time series indicate the missing data. (b-d) Vertical profiles of potential temperature (θ), normalized vertical velocity variance ($\sigma_w^2\, w_*^{-2}$), particle total surface area (Stot), and water vapor mixing ratio (MR).

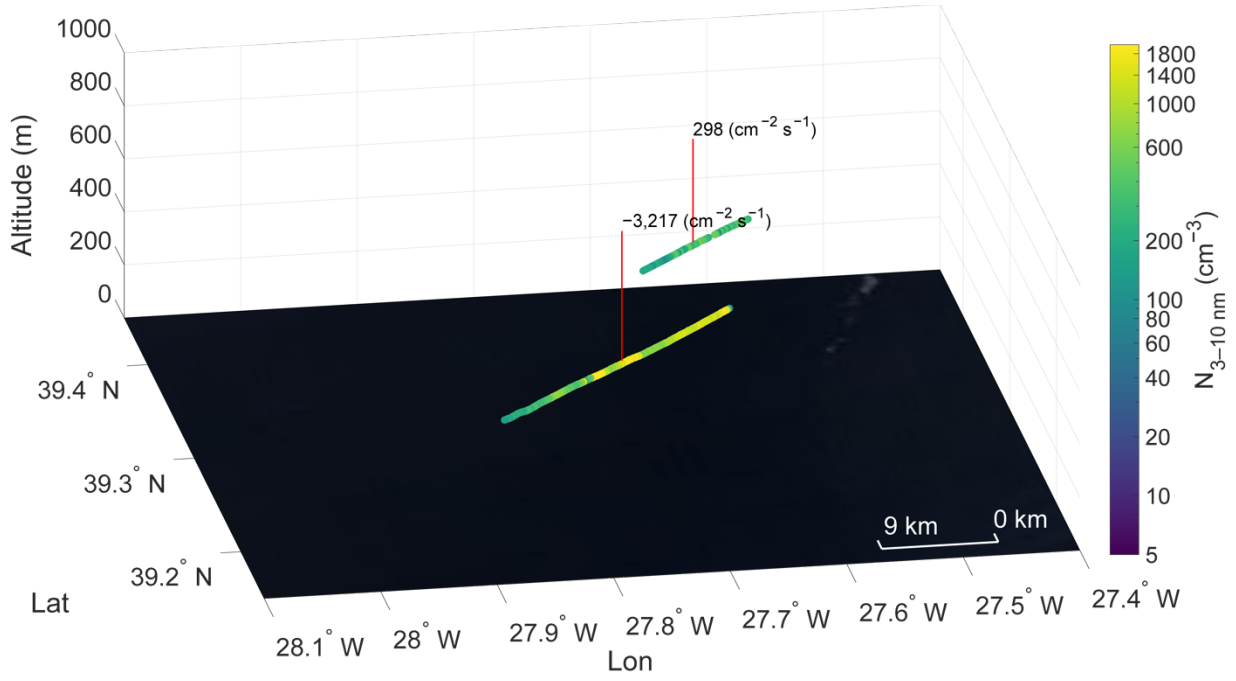

Figure S15. Spatial distribution of $N_{3–10}$ particle concentrations along the flight track during the period highlighted in pink in Figures S13 and S14. Mean calculated fluxes are labeled on the track. Color scale indicates particle number concentrations (cm^{-3}). The background shows a satellite-corrected reflectance image taken from the overpass at 14:50 UTC with the ocean surface appearing dark and clouds appearing white, Credit: NASA Worldview Snapshots.

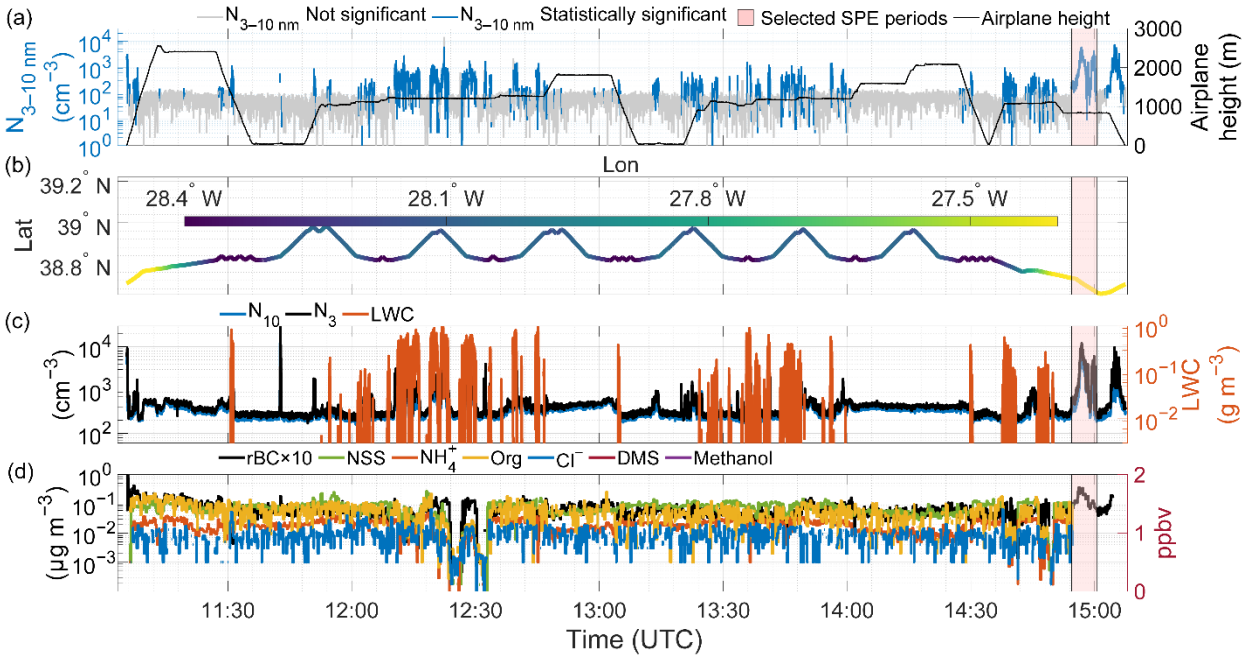

Figure S16. Multi–parameter time series analysis during the February 12, 2018 flight showing: (a) $N_{3–10}$ particle concentrations with aircraft altitude; (b) aircraft position showing latitude and longitude; (c) particle number concentrations for N_{10}, N_3, and liquid water content (LWC); and (d) non-refractory aerosol chemical composition including non–seasalt sulfate (NSS), ammonium ion (NH_4^+), organics (Org), and chlorine ion (Cl^-), plus refractory black carbon (rBC, multiplied by 10 for visualization) in μg m^{-3}, and trace gas concentrations of dimethylsulfide (DMS) and methanol in ppbv.

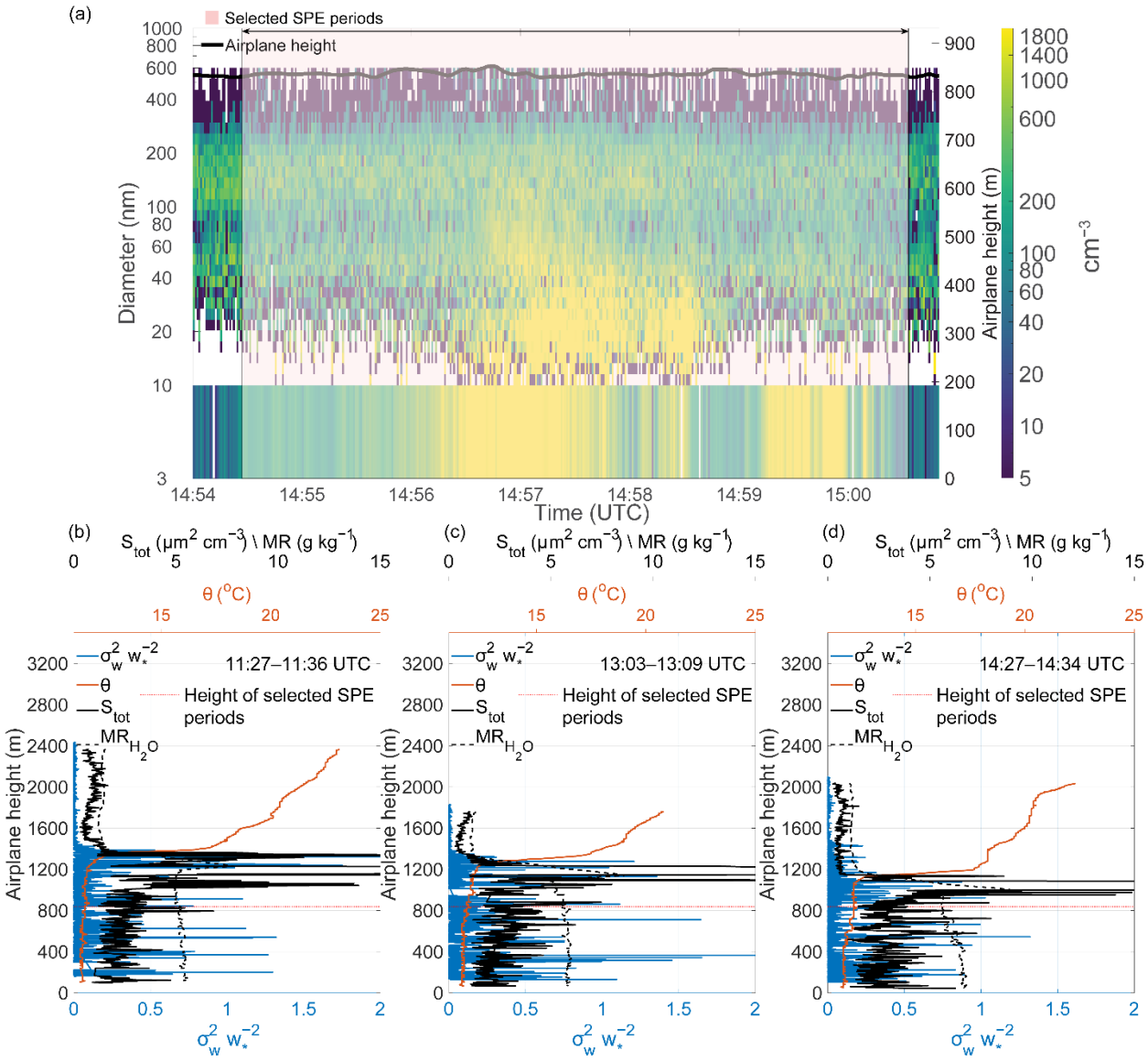

Figure S17. (a) The main panel shows size-resolved particle number concentrations (10–600 nm diameter) from FIMS as a function of time and altitude, while $N_{3–10}$ concentrations are displayed in the lower strip. Colors represent particle number concentrations (cm^{-3}) according to the scale bar. Gaps in the time series indicate the missing data. (b-d) Vertical profiles of potential temperature (θ), normalized vertical velocity variance ($\sigma_w^2\, w_*^{-2}$), particle total surface area (Stot), and water vapor mixing ratio (MR).

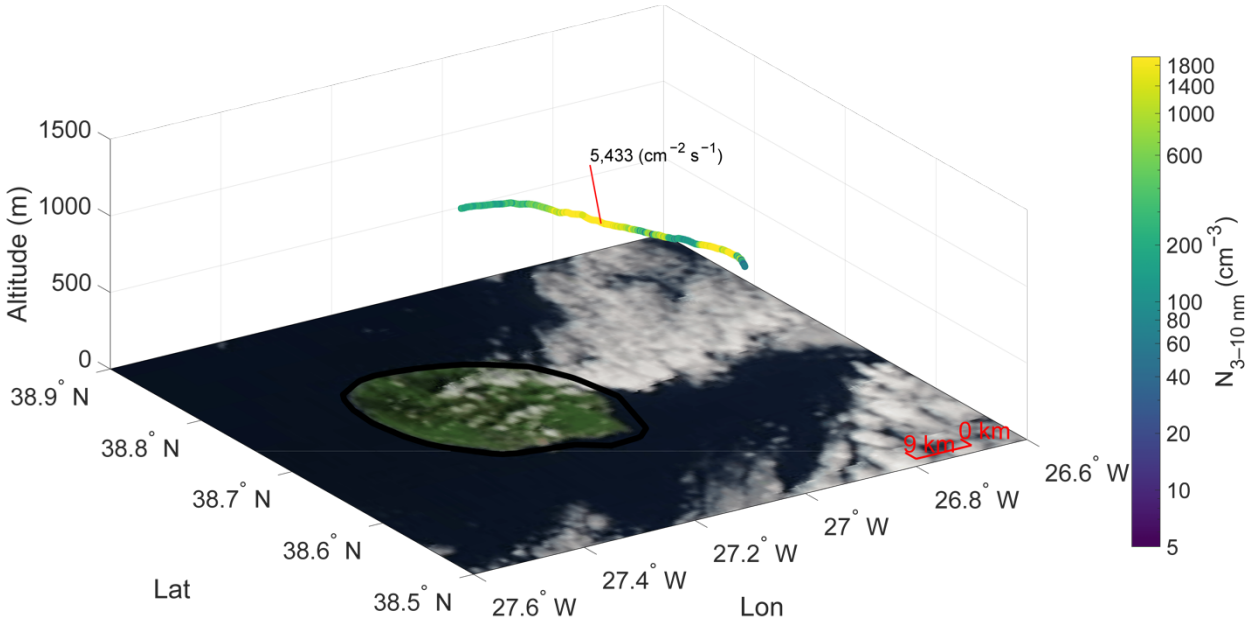

Figure S18. Spatial distribution of $N_{3\text{-}10}$ particle concentrations along the flight track during the period highlighted in Figures S16 and S17. Mean calculated fluxes are labeled on the track. Color scale indicates particle number concentrations (cm^{-3}). The background shows a satellite-corrected reflectance image taken from the overpass at 15:27 UTC, with the ocean surface appearing dark and clouds appearing white, Credit: NASA Worldview Snapshots.